Correlation of Heat Transport and Shear Forces in Nanoscale Junctions

B. J. Robinson, M. E. Pumarol, and O. V. Kolosov*

Physics Department, Lancaster University, Lancaster, LA1 4YB, UK
Correspondence to be addressed to: o.kolosov@lancaster.ac.uk, WWW: http://www.nano-science.com/

Nanoscale solid-solid contacts define a wealth of materials behaviour from the friction in micro- and nanoelectromechanical systems[1] to electrical and thermal conductivity in modern electronic devices[2]. For modern, ultra-high integration processor chips and power electronic devices one of most essential, but thus far most challenging, aspects is the heat transport in nanoscale sized interfaces[3]. Highest spatial resolution to date, achieved via nanoscale probes in scanning thermal microscopy (SThM)[4], is often devalued by the poorly defined nature of the nanoscale contacts[5]. Here we show that simultaneous measurement of shear forces and heat flow between the probe and the studied material elucidates the key parameters of solid-solid contact. Our analysis indicates the intrinsic ballistic nature of heat transport via nanoscale contacts in such a system. Furthermore, in analogy to the Wiedemann-Franz law linking electrical and thermal conductivity in metals[6], we show that a generalised relation exists linking shear forces and thermal resistance in nanoscale contacts via fundamental material properties such as heat capacity and heat carrier group velocity. These factors, together with the clearly observed anti-correlation of the thermal resistance and shear forces, demonstrate a quantitative approach for the experimental characterisation of thermal transport in nanoscale junctions.

As continuously decreasing length scales are being exploited in electronic devices, nanoelectromechanical systems and nanomaterials, understanding the true nature of nanoscale contacts between solid surfaces and interfaces is essential. Whilst electron transport[7] and force interaction[8] in such contacts have been well explored, studying nanoscale heat transport in active (heat generating) and passive (heat dissipating) nanostructures[9] still poses significant challenge. This is further complicated as the critical dimensions of these in modern devices continue to decrease below the mean free path (MFP) of electrons and phonons – the two major types of heat carriers in solid state devices[10].

A leading instrument for nanoscale thermal mapping, SThM, relies on the heat transfer between a nanometre dimension apex of a heated thermal probe[11] and the studied sample, the resulting change of the probe temperature on contact with the sample allowing estimation of its local thermal conductivity[12,13]. Unfortunately, due to generally irregular and fluctuating morphology of the nanoscale solid-solid contact (shown schematically in Fig. 1), these phenomena are difficult to model and even more difficult to experimentally investigate therefore significantly reducing the reliability and effectiveness of nanoscale heat transport SThM measurements[14].
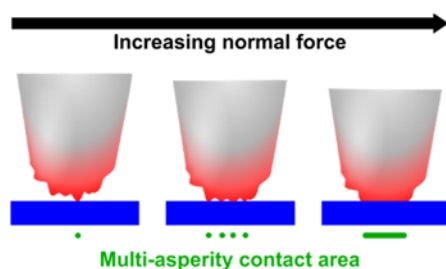

Figure 1 | Multi-asperity contact between a heated SThM probe and sample. Schematic diagram showing how contact area (green line) between probe and sample does not increase linearly due to the unpredictable and fluctuating nature of the probe-sample nanoscale interface.

A tempting approach to resolve this, would be to find another parameter complimentary to the heat transfer, sensitive to the state of the nanoscale junction. Recent reports[5] that link heat transport in nanoscale junctions and the normal force, together with well-established dependence of friction force on the normal force, and hence solid-solid contact area[15-17] prompted us to make simultaneous measurements of the shear force and the heat transport. Another potentially useful measurement – a tip-surface compliance would require reliable determination of high values on the order of several 1000 N m^{-1} by, e.g. ultrasonic force microscopy[18], that is generally harder to quantify and therefore we did not use this approach here. With normal force acting as an external parameter influencing both heat transport and shear stresses it becomes possible to eliminate the biggest unknown of a nanoscale contact – its true dimension. Simultaneous measurements of thermal response, normal and shear forces during tip-surface approach (see Methods) shown in Fig. 2 clearly showing that both thermal (curve a) and shear (curve c) response have a strong dependence on the normal force that is almost perfectly linearly depend on the sample-tip approach (curve b).
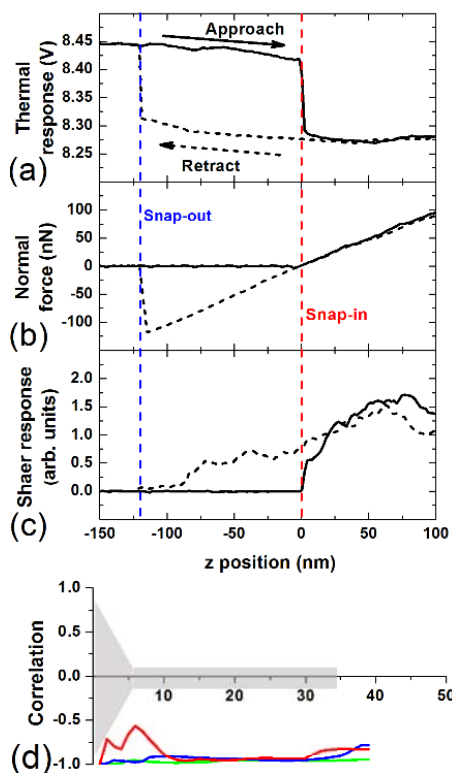
Figure 2 | Typical experimental single parameter investigation of probe-sample contact. a, thermal response, **b**, normal force and **c**, shear response as a function of relative cantilever displacement (*z* - position) of SThM probe on a polished quartz substrate. In each case the *z* position is zeroed at the surface of the sample; solid line is corresponds to cantilever approach and dashed line to cantilever retraction. All curves clearly indicate the onset (red line) and breaking (blue line) of the solid-solid contact, the fine features of the thermal contact fluctuations in are practically not observable in the normal force response. **d**, Correlation analysis (from 5 to 50 nm) between experimental thermal and shear responses, where the grey shaded region corresponds to simulated random responses (see Supplementary Note 2).

The pilot experiments to exploit simultaneous measurement of heat transport and contact shear strength in nanoscale contacts were performed in ambient conditions on a 100 nm Au-coated polished quartz substrate (Supplementary Note 1). A micro-fabricated Si_3N_4 thermal probe (SP, see Methods) was slowly at 10 nm s^{-1}, brought into contact with the sample in the standard force spectroscopy way[19]. Remarkably, the behaviour of the thermal resistance and shear response was clearly opposite, quantitatively supported by the correlation analysis of these curves. The correlation coefficient in the range of − 1 to − 0.8

(Fig. 2d) was well above the level of $\pm$ 0.15 for the typical shear force and thermal signals correlated with simulated noise (Supplementary Note 2).

We then conducted detailed SThM studies in air and high vacuum (1×10^{-7} Torr) environment to investigate the relative contributions to the nanoscale heat transfer phenomena at the tip-sample contact. These could be a) solid-solid contact of the probe apex and the sample[20], b) through-the-air conduction[21], c) heat transfer via liquid bridge of condensed water in the contact region[22], and d) radiative far-field and near-field heat transfer with a latter being negligible in measurement conditions[4]. Here a doped Si (DS, see methods) microfabricated probe was brought into contact with polished Si surface and, as above, monitored for both thermal response and shear response during approach-retract cycles, Fig. 3.
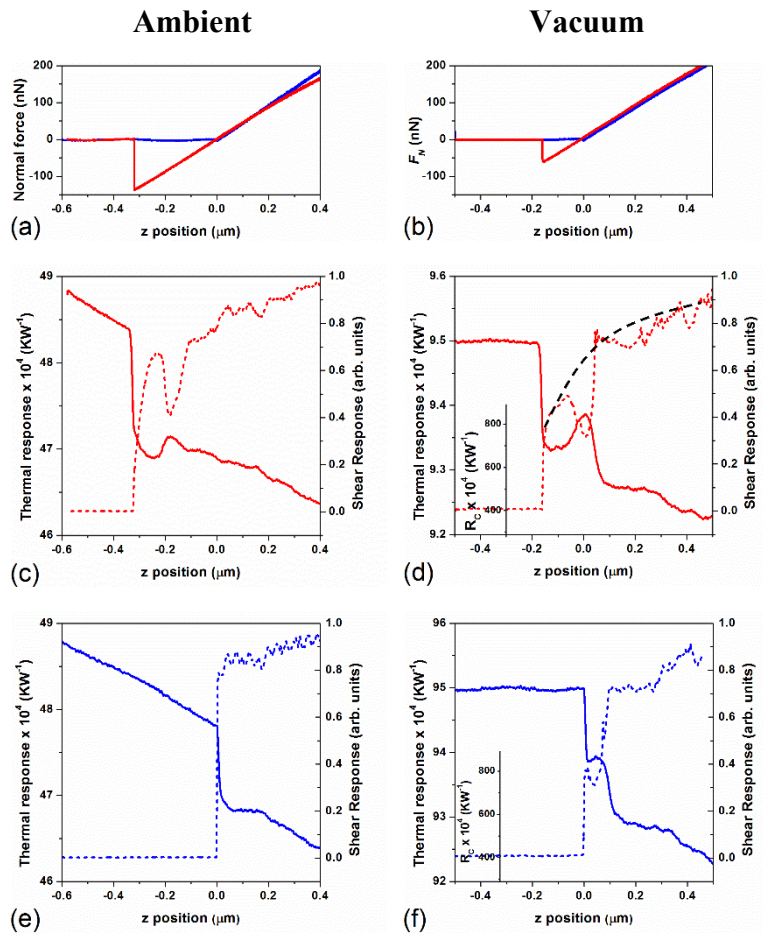
Figure 3 | Comparison of thermal and shear responses in ambient and vacuum environments. Approach-retract cycles in (**a, c, e**) ambient and (**b, d, f**) vacuum environments using DS probe. **c-f**, Simultaneous total thermal resistance (solid lines) and lateral force (dashed lines) signals obtained during tip retracting from (**c, d**) and approaching to (**d ,f**) to the surface (insert corresponds to contact thermal resistance R_C). While normal forces show little if any correlation with the thermal response, shear forces show clear anti-correlation with the thermal responses. Shear response presented reflects the friction shear force between probe and sample, acquired via lateral dithering of the sample perpendicular to the long axis of the cantilever and observing resulting torsion of the cantilever.

The thermal response gradient, as the tip approaches the surface, associated with gas conduction of heat from the cantilever to the surface is observed in air (Fig. 3e) but is fully

eliminated in high vacuum environment (Fig. 3f). Furthermore, whilst there is significantly greater adhesion due to the presence of the tip-sample water bridge (~137 nN in air and ~62 nN in vacuum) we observed negligible qualitative differences between the change in thermal response directly associated with tip snap-in and, crucially, snap-out, suggesting that this via-the-meniscus heat condition channel is less significant than previously thought[4,23] and that the major contributing factor to the heat transfer arises from the solid-solid contact of the probe apex and the sample.

For a simplest case of single asperity solid-solid contact, the relation between cantilever deflection, and probe-sample contact area is relatively well understood[24] (see also Methods) and is dependent upon the contact formed by the probe's radius of curvature (r) and the applied normal force or load (L). It can be shown that, in vacuum, shear response[25], or friction force (F_f) and ballistic limit thermal resistance (R_{Cb})[26] in case of predominantly phonon heat transport between similar materials is related directly to the *actual* contact area (A=πa²) between the probe and sample such that,

$$R_{Cb} = \frac{4}{C v_g \pi a^2} \text{ and } F_f = \tau \pi a^2$$

Where C is the specific heat capacity per unit volume and v_g is the phonon group velocity (here 1.66 × 10⁶ J/m³ K and 6400 m/s respectively)[27], τ interfacial shear strength for single asperity contact of radius a. In the diffusive limit (a ~ l), the thermal resistance is given by $R_{Cd} = 1/2ka.$ The behaviour of these models as a function of r, and L is shown in Supplementary note 3.

We compared the experimental and modelled vacuum SThM response (Fig 3. d,f) as the ratio of shear and thermal responses as a function of r, in both ballistic (Fig. 4 a) and diffusive (Fig. 4 b) approximations. Here the shear response has been normalised to the range

0-1 for the same maximum load (0 equivalent to absence of friction immediately prior to snap in to contact and, here, 1 equivalent to F_f at L = 150 nN) to allow direct inter-comparison between series of measurements without the need to fully characterise the shear strength τ.
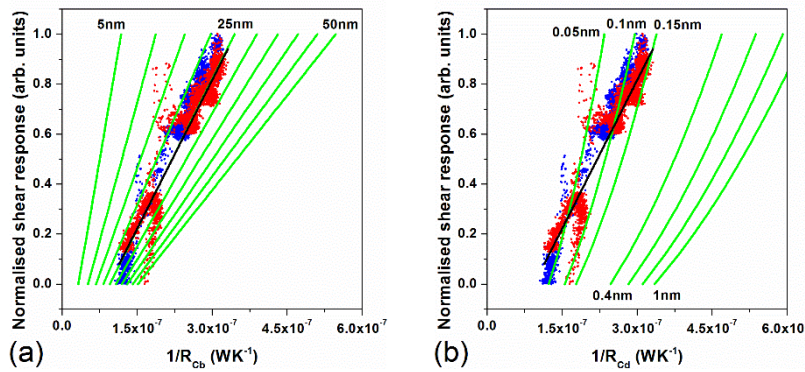

Figure 4 | Comparison of experimental and modelling shear and thermal responses. Experimental approach (blue) and retract (red) data and modelling (green) for single asperity contacts in **a**, the ballistic and **b**, diffusive thermal limits. A black line is a linear fit to the average of the experimental data, green lines show the modelling data for a series of single asperity contacts incremented in the range r = 5-50 nm for R_{Cb} and at values r = 0.05, 0.1, 0.15 and 0.4-1nm R_{Cd}.

In the ballistic limit the total contact area between probe and sample corresponds to the equivalent of a single asperity contact formed by a probe of r = 25 nm which corresponds with the manufacturers stated value of r < 30 nm (see Methods). Assuming the diffusive heat transport approximation, the experimental data could only be approximated at single point for r ~ 0.1 nm, which is physically unrealistic with the SThM probes used. Critically, knowing the value of r allows the calculation of contact area A for each point in the experimental data.

It should be noted that the experimental ratio in Fig. 4, whilst generally linear, has significant scatter and some branching suggesting that the probe does not interact with the sample as an ideal single asperity contact. This corresponds with the non-monotonous nature of both the shear and thermal response (see eg. variation against guide to the eye) in Fig. 3d,f

and may be further investigated using a multi-asperity contact model using, for example, molecular dynamic simulations[28].

For the single asperity case, in an analogy to the as the Wiedemann–Franz law describing the relationship between the thermal conductivity and electrical conductivity of a metal [29], here we can relate the thermal contact resistance with the normalised shear force F_f/τ in a nanoscale contact between similar materials via fundamental parameters of group velocity and heat capacity

$$R_{cb} = \frac{4}{Cv_g} \cdot \left(\frac{F_f}{\tau}\right)^{-1}$$

Crucially, as nanoscale junction operates in the ballistic limit of thermal transport, the mean free path of phonons need not be considered. Moreover, as the total area governs both heat transport and shear forces, this relation should be equally valid for the generic case of multi-asperity contact.

In conclusion, we elucidate heat transport in nanoscale solid-solid contacts by simultaneous monitoring of shear forces and the heat transport in the scanning thermal microscopy based approach. We observed a clear inverse correlation between the thermal resistance and shear forces at varying normal load with a correlation coefficient close to negative 1. Our comparative analysis suggests that the heat transport in these typical nanoscale solid-solid contacts is of ballistic nature via single or multi-asperities contact. Moreover, we were able to propose a generalised relationship between shear response and ballistic thermal resistance for nanoscale contacts which can be easily realised in practically any nanoscale contact pairs having phonon dominated heat transport and may play a significant role in improving the quality and reliability of measurement of nanoscale thermophysical properties and development of nanoelectromechanical systems.

Methods

SPM measurements. Ambient SThM measurements were performed using a standard contact AFM steup (Bruker Multi-Mode, Nanoscope III) with 'half-moon' SThM probe holder (Anasys Instruments) using a Pd heater (SP) probe (Kelvin Nanotechnologies). 1×10^{-7} mBar high vacuum (HV) measurements were performed in a dedicated low vibration chamber using a HV compatible AFM (NT-MDT Smena multimode SPM) and doped Si probe (DS) (AN-200, Anasys Instruments). In both cases, during measurement, the thermal probe represents part of a balanced Maxwell electric bridge with a 4 V_{AC} signal at 91 kHz frequency, provided by a precision function generator (Model 3390, Keithley instruments), used for resistance measurements and a DC offset providing probe Joule self-heating [30]. The probe's electrical resistance was recorded as a function of applied voltage and temperature as using the method described elsewhere[13]. A shear piezo actuator (Physik Instrumente, PI-121.03) was used to laterally oscillate (70 Hz and a drive voltage of 0-5 V) the sample perpendicular to the longitudinal axis of the cantilever during probe approach-retract, in-phase (x) and out-phase (y) component of the friction response were recorded by an additional lock-in amplifier (as above).

Probe specifications. SP probe (Kelvin Nanotechnology), is made of low thermal conductivity silicon oxide (k_{SP} ~ 1Wm^{-1}K^{-1}) and has a Pd resistive temperature sensor that is positioned at the apex of the tip. Manufacturers stated tip radius is <100 nm but is typically found to be ca. 50 nm. DS probes (Anasys Instruments), are made of single crystal Si of high thermal conductivity (k_{DS} ~ 1Wm^{-1}K^{-1}) and a small radius of curvature of the tip of approximately <30

nm The moderately doped resistive temperature sensing part of this probe is separated from the tip apex by the end section of the cantilever and height of the probe tip itself.

Calculation of actual contact area. The actual contact area can be calculated using the JKR model[24] such that the variation of a with normal force equivalent load (L) is given by $a/a_0 = ((1 + \sqrt{(1 - L/L_c)})/2)^{\frac{2}{3}}$ where L_c is the negative critical load. L is derived from z-displacement using Hooke's law in the standard way[19], L_c can be experimentally determined as the pull off force of the probe from the sample and a_o is the contact radius at zero load such that $a_0 = ((6\pi\gamma r^2)/K)^{\frac{1}{3}}$ where r is the tip curvature radius, γ is interfacial energy per unit area (work of adhesion) and K is the combined elastic modulus of tip and sample such that $K = 4/3 ((1 - v_1^2)/E_1 + (1 - v_2^2)/E_2)$ where E_1 and E_2 are the Young's moduli of tip and sample respectively and v_1, v_2 are Poisson ratios of the tip and sample respectively. Here E_{SiO2} = 55 GPa and v_{SiO2} = 0.27 [8]. γ can be calculated directly from experimental measurement of L_c such that $L_c = -\frac{3}{2}\pi\gamma r$ such that simulation can be pinned directly to the experimental results through the pull-off force of the probe from the sample reducing errors which may arise from, for example, surface contamination of the sample which could significantly change the value of γ. In this way, for our system comprising Si in vacuum, we calculate γ in the range 2.589 – 0.259 Jm^{-2} for $r = 5 – 50$ nm, which compares to 0.34 Jm^{-2} previously reported for $r =$ 10 nm in ambient conditions[8]. In summary r and L_c allow the calculation of γ and a_0 which then allows the calculation of a for different values of L. Here we derive L and L_c from experiment and treat r as a variable.

Calculation of shear response. Friction response is given by $F_f = \tau A$ where τ is the constant interfacial shear strength[15]. Assuming geometrical symmetry between a conical tip – planar

sample, contact can be modelled as circular constriction such that for a single asperity contact such that $A=\pi a^2$ and $F_f = \tau \pi a^2$.

Calculation of thermal response. Thermal resistance of the probe-sample interface can be calculated using the method outlined by Prasher[26] which considers a general solution, defined by the Knudsen number (l/a) for both the diffusive (a » l) and ballistic (a ~ l) where l is the mean free path of phonons in the material. The thermal contact resistance (R_c) can be written as $R_c = \frac{1}{2}ka\left[1 + \frac{8}{3\pi}Kn\right]$ where $k = \frac{1}{3}Cv_g l$ and C is the specific heat capacity per unit volume and v_g is the phonon group velocity[27]. In the ballistic approximation, we assume that $Kn \rightarrow \infty$ and for ballistic heat flow regime $R_{Cb} = 4l/3k\pi a^2$ and in the diffusive limit ($Kn \rightarrow 0$), the thermal resistance is given by $R_{Cd} = 1/2ka$.

Author's contibutions.

O.V.K. conceived the idea of the approach, B.J.R, M.P and O.V.K performed the experiments, B.J.R and O.V.K provided the analysis of the experimental data and the analytical modelling, B.J.R and O.V.K prepared the manuscript.

Conflict of interests.

Authors declare no conflict of interests.

References.

1   Nikhil, S. T. & Bharat, B. Scale dependence of micro/nano-friction and adhesion of MEMS/NEMS materials, coatings and lubricants. *Nanotechnology* **15**, 1561 (2004).

2   Pernot, G. *et al.* Precise control of thermal conductivity at the nanoscale through individual phonon-scattering barriers. *Nat Mater* **9**, 491-495, doi:http://www.nature.com/nmat/journal/v9/n6/suppinfo/nmat2752_S1.html (2010).

3   Hoogeboom-Pot, K. M. *et al.* A new regime of nanoscale thermal transport: Collective diffusion increases dissipation efficiency. *Proceedings of the National Academy of Sciences* **112**, 4846-4851, doi:10.1073/pnas.1503449112 (2015).

4   Gomès, S., Assy, A. & Chapuis, P.-O. Scanning thermal microscopy: A review. *physica status solidi (a)* **212**, 477-494, doi:10.1002/pssa.201400360 (2015).

5   Gotsmann, B. & Lantz, M. A. Quantized thermal transport across contacts of rough surfaces. *Nat Mater* **12**, 59-65, doi:http://www.nature.com/nmat/journal/v12/n1/abs/nmat3460.html#supplementary-information (2013).

6   Franz, R. & Wiedemann, G. Ueber die Wärme-Leitungsfähigkeit der Metalle. *Annalen der Physik* **165**, 497-531, doi:10.1002/andp.18531650802 (1853).

7   Lambert, C. J. Basic concepts of quantum interference and electron transport in single-molecule electronics. *Chem. Soc. Rev.* **44**, 875-888, doi:10.1039/C4CS00203B (2015).

8   Robinson, B. J. & Kolosov, O. V. Probing nanoscale graphene-liquid interfacial interactions via ultrasonic force spectroscopy. *Nanoscale* **6**, 10806-10816, doi:10.1039/c4nr01348d (2014).

9   Pop, E. Energy Dissipation and Transport in Nanoscale Devices. *Nano Research* **3**, 147-169, doi:10.1007/s12274-010-1019-z (2010).

10   Johnson, J. A. *et al.* Direct Measurement of Room-Temperature Nondiffusive Thermal Transport Over Micron Distances in a Silicon Membrane. *Physical Review Letters* **110**, 025901 (2013).

11   Shi, L. & Majumdar, A. Thermal transport mechanisms at nanoscale point contacts. *Journal of Heat Transfer-Transactions of the Asme* **124**, 329-337, doi:10.1116/1.1447939 (2002).

12   Hinz, M., Marti, O., Gotsmann, B., Lantz, M. A. & Durig, U. High resolution vacuum scanning thermal microscopy of HfO2 and SiO2. *Applied Physics Letters* **92**, 3, doi:043122

10.1063/1.2840186 (2008).

13   Pumarol, M. E. *et al.* Direct Nanoscale Imaging of Ballistic and Diffusive Thermal Transport in Graphene Nanostructures. *Nano Lett.* **12**, 2906-2911, doi:10.1021/nl3004946 (2012).

14   Cahill, D. G. *et al.* Nanoscale thermal transport. II. 2003–2012. *Applied Physics Reviews* **1**, -, doi:doi:http://dx.doi.org/10.1063/1.4832615 (2014).

15   Carpick, R. W. & Salmeron, M. Scratching the surface: Fundamental investigations of tribology with atomic force microscopy. *Chem. Rev.* **97**, 1163-1194, doi:10.1021/cr960068q (1997).

16   Bhushan, B. Nanotribology and nanomechanics. *Wear* **259**, 1507-1531, doi:10.1016/j.wear.2005.01.010 (2005).

17   Robinson, B. J., Kay, N. D. & Kolosov, O. V. Nanoscale Interfacial Interactions of Graphene with Polar and Nonpolar Liquids. *Langmuir* **29**, 7735-7742, doi:10.1021/la400955c (2013).

18   Dinelli, F., Biswas, S. K., Briggs, G. A. D. & Kolosov, O. V. Measurements of stiff-material compliance on the nanoscale using ultrasonic force microscopy. *Physical Review B* **61**, 13995-14006 (2000).

19   Butt, H.-J., Cappella, B. & Kappl, M. Force measurements with the atomic force microscope: Technique, interpretation and applications. *Surf. Sci. Rep.* **59**, 1-152, doi:10.1016/j.surfrep.2005.08.003 (2005).

20   Cahill, D. G. *et al.* Nanoscale thermal transport. *Journal of Applied Physics* **93**, 793-818, doi:10.1063/1.1524305 (2003).

21   Lefèvre, S., Volz, S. & Chapuis, P.-O. Nanoscale heat transfer at contact between a hot tip and a substrate. *Int. J. Heat Mass Transfer* **49**, 251-258, doi:http://dx.doi.org/10.1016/j.ijheatmasstransfer.2005.07.010 (2006).

22   Luo, K., Shi, Z., Varesi, J. & Majumdar, A. Sensor nanofabrication, performance, and conduction mechanisms in scanning thermal microscopy. *J. Vac. Sci. Technol. B* **15**, 349-360, doi:10.1116/1.589319 (1997).

23   Majumdar, A. Scanning thermal microscopy. *Annu. Rev. Mater. Sci.* **29**, 505-585 (1999).

24   Carpick, R. W., Ogletree, D. F. & Salmeron, M. A general equation for fitting contact area and friction vs load measurements. *Journal of Colloid and Interface Science* **211**, 395-400, doi:10.1006/jcis.1998.6027 (1999).

25   Schwarz, U. D., Zworner, O., Koster, P. & Wiesendanger, R. Quantitative analysis of the frictional properties of solid materials at low loads .1. Carbon compounds. *Physical Review B* **56**, 6987-6996, doi:10.1103/PhysRevB.56.6987 (1997).

26   Prasher, R. Predicting the thermal resistance of nanosized constrictions. *Nano Letters* **5**, 2155-2159, doi:10.1021/nl051710b (2005).

27   Chen, G. Thermal conductivity and ballistic-phonon transport in the cross-plane direction of superlattices. *Physical Review B* **57**, 14958-14973 (1998).

28   Mo, Y., Turner, K. T. & Szlufarska, I. Friction laws at the nanoscale. *Nature* **457**, 1116-1119, doi:http://www.nature.com/nature/journal/v457/n7233/suppinfo/nature07748_S1.html (2009).

29   Wilson, R. B. & Cahill, D. G. Experimental Validation of the Interfacial Form of the Wiedemann-Franz Law. *Phys. Rev. Lett.* **108**, 255901 (2012).

30   Tovee, P., Pumarol, M. E., Zeze, D. A., Kjoller, K. & Kolosov, O. Nanoscale spatial resolution probes for Scanning Thermal Microscopy of solid state materials. *J. Appl. Phys.* **112**, 114317 (2012).

Correlation of Heat Transport and Shear Forces in Nanoscale Junctions

B. J. Robinson, M. E. Pumarol, and O. V. Kolosov*

Supplementary note 1: Analysis of probe approach in ambient conditions

During approach of the heated SThM probe, in ambient conditions, a sharp snap-in to contact occurs when the gradient of attractive forces, predominantly van der Waals and water capillary bridging[1], between sample and probe is greater than the cantilever spring constant, k (at k_{SP} ~0.3 Nm^{-1}). Simultaneously, a sharp decrease in thermal response at the surface (z position of 0 nm) arises from conductance between the heated probe and sample due to the onset of solid-solid contact. The gradient of the thermal response prior to snap-in (negative z position) is due to conduction through the narrowing probe-sample air gap[1,2]. For Au surface, immediately after the contact, the probe temperature decreases indicating decrease of the thermal resistance of the probe, due to increase of the contact area following the increase of the normal force. Simultaneously, the friction force that was zero shear prior to solid-solid contact, increases close to monotonous dependence after the initial contact with the increase of the load[3]. It should be noted that for SiO2 sample, both the thermal and shear response post contact are far from being monotonous (arrows in Fig.S1a) that may be linked with the probe tilt and constant torsion under normal forces, so that a different zone of the probe apex is contacting the surface. We noted no change in response over multiple (~100) cycles indicating negligible wear of the probe or sample.
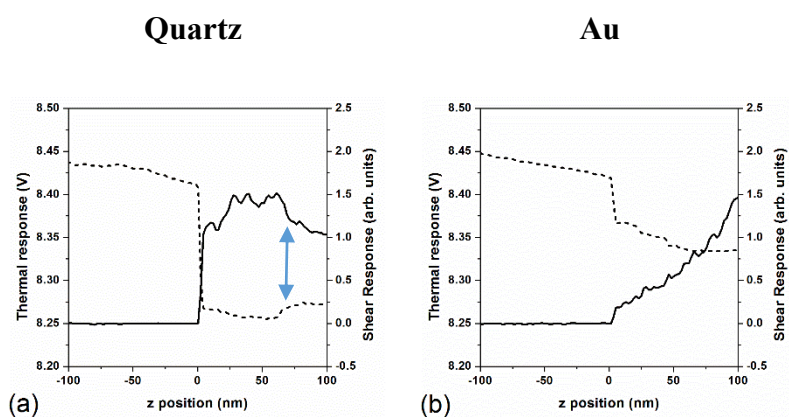
Quartz   **Au**

(a)   (b)

Figure S1 | Comparison of Au and Quartz thermal and shear responses. Two representative thermal (dashed lines) and shear (solid lines) responses of a nanoscale *SP* SThM probe approaching **a**, quartz and **b**, Au surfaces (z=0 corresponds to the sample surface).

Supplementary note 2: Correlation analysis of thermal and shear responses

Correlation analysis, using the Pearson product-moment correlation coefficient, was performed on the multiple sets of experimental data of the thermal response and shear response for both Quartz and Au, typical responses for which are shown in Fig. S1. In each case a correlation coefficient between -1 and +1 is generated where -1 indicates a perfect negative correlation, +1 indicates a perfect positive correlation and coefficients around 0 indicates no correlation.

Here we compared experimental thermal data with randomly generated shear data (Fig. S2a,b) of the same overall mean value and maximum/minimum values. Similarly, we compared experimental shear data with randomly generated thermal data (Fig S2c,d). In both cases coefficients were typically in the range of ± 0.15. Correlation coefficients between experimental shear and experimental thermal responses were in the range − 1 to − 0.8 (Fig. S2e,f).
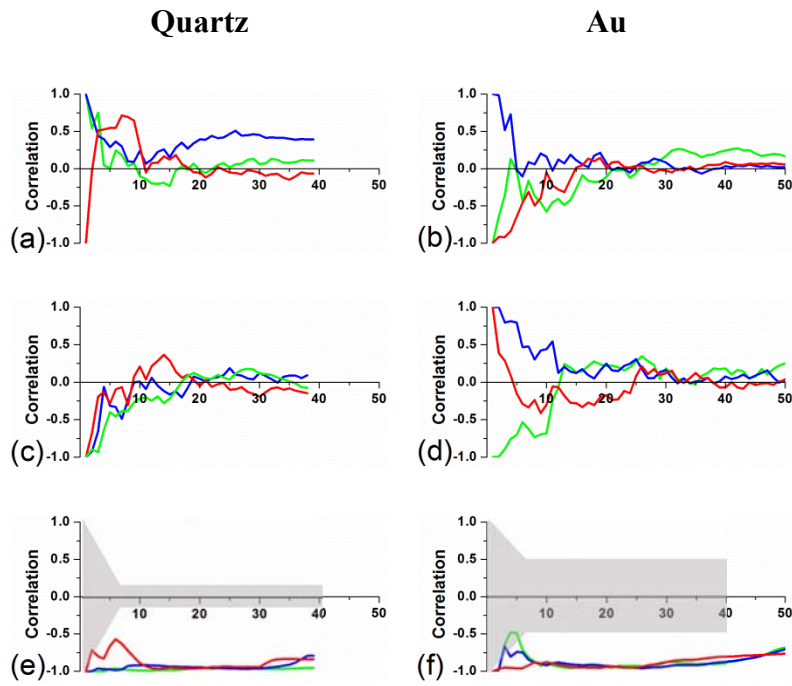
Quartz **Au**

Figure S2 | Correlation analysis of simulated and real shear and thermal responses. a, b experimental thermal response data vs random distribution shear response data for quartz and Au respectively. **c, d** experimental shear response data vs random distribution thermal response data for quartz and Au respectively. **e, f** correlation of experimental data for both shear and thermal responses demonstrating a correlation coefficient in the range -0.8 to -1.0. In all cases correlation is calculated on the solid-solid contact regime corresponding to z position of 5 to 50 nm.

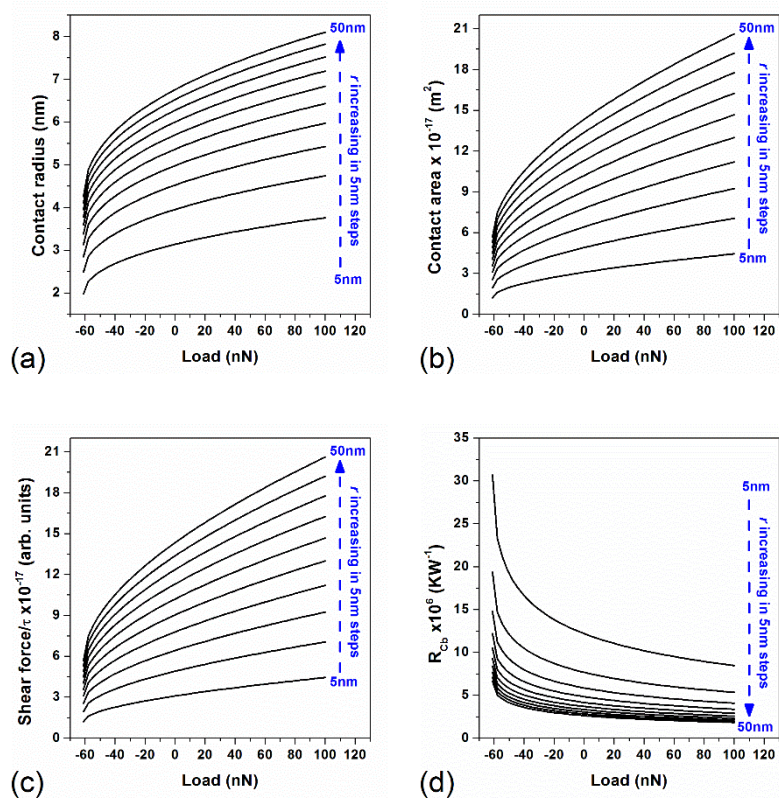# Supplementary note 3: Modelling of shear and thermal responses

Figure S3 | Modelling of actual contact, shear and thermal responses in vacuum. Calculated **a**, actual contact radius **b**, actual contact area **c**, shear force/τ and **d**, contact thermal resistance in the assumption of ballistic heat transport (R_{Cb}), corresponding to the experimental system in vacuum as function of load L for a probe radius of curvature r.

1   Shi, L. & Majumdar, A. Thermal transport mechanisms at nanoscale point contacts. *Journal of Heat Transfer-Transactions of the Asme* **124**, 329-337 (2002).

2   Gomès, S., Assy, A. & Chapuis, P.-O. Scanning thermal microscopy: A review. *physica status solidi (a)* **212**, 477-494 (2015).

3   Franzka, S. & Zum Gahr, K. H. Microtribological studies of unlubricated sliding Si/Si contact in air using AFM/FFM. *Tribology Letters* **2**, 207-220 (1996).